Leszek Jarecki, Andrzej Ziabicki

Institute of Fundamental Technological Research Polish Academy of Sciences
Świętokrzyska 21, 00-049 Warsaw, Poland
E-mail: ljarecki@ippt.gov.pl, aziab@ippt.gov.pl

Mathematical Modelling of the Pneumatic Melt Spinning of Isotactic Polypropylene Part II. Dynamic Model of Melt Blowing

Abstract
A single-, thin-filament model for stationary melt blowing of nonwovens from isotactic polypropylene is proposed. The Phan-Thien and Tanner constitutive equation of viscoelasticity is used, as well as the effects of stress-induced crystallisation on polymer viscosity and relaxation time during the processing are accounted for. The predetermined air velocity, temperature and pressure fields are assumed, which are computed for different initial air velocities as well as a fixed initial temperature, and approximated along the melt blowing axis by analytical fit formulae. The model is more general and can be applied to the melt blowing of nonwovens from other crystallising polymers and other air fields. The axial profiles of polymer velocity, temperature, tensile stress, pressure, amorphous molecular orientation and the degree of crystallinity can be computed using the model presented.

Keywords: *melt blowing of nonwovens; modelling of melt air-drawing; dynamic functions in melt air-drawing; air jet dynamics in melt blowing.*

Introduction

Fundamental equations of the fiber melt spinning processes proposed by Ziabicki [1-4], Andrews [5], and Kase [6-8] in the 1960s, further developed and modified next by other authors [9-15], are used for the modelling of the pneumatic process in non-woven melt blowing. Computer aided mathematical modelling offers an alternative method to costly experimental investigations, which is expected to provide valuable information on the process dynamics and role of individual processing parameters. The modelling presented in our paper concerns pneumatic melt spinning with isotactic polypropylene. The models of the pneumatic process presented by other authors [16, 17] who considered the melt blowing of polypropylene non-woven did not take polymer viscoelasticity into account, which is important in the case of polyolefines. They reported that the diameters of fibers above 50 μm computed using the modelling are in agreement with the experimental data presented in [18] for rather thick fibers. In melt blowing, the main attenuation of filaments takes place near the spinneret, within a distance range of about 6 cm [18], and next the filaments are collected on a take-up device at a distance of several tens of centimeters.

In the pneumatic process we deal with the dynamic interactions between two phases – the polymer melt extruded from a single row of orifices evenly distributed in a longitudinal spinneret beam and convergent air jets blown symmetrically from a dual slot die onto both sides of polymer filaments. The filaments and the air jets interact three dimensionally, where the system exhibits a symmetry plane determined by the row of filaments blown along the centerline of the air jets from the beam. The dynamics of the melt blowing process is controlled by the velocity, temperature and pressure fields of the air jets. Difficulties in determining the fields are related to the formulation of the boundary conditions between the phases.

Usually, models of melt spinning processes consider the velocity and temperature fields separately for a polymer and gaseous medium. Such separation is also assumed for the pneumatic process where the stationary velocity, temperature, and pressure fields of the convergent air jets were predetermined in Part I of the publication series [19] as well as presented in [20]. Dynamic fields were computed for several initial air velocities between 30 and 300 m/s at the output of the slots, at a fixed initial air temperature of 300 °C. We assume that the air conditions can be approximated by predetermined air jet fields for melt blowing processes with a single row of filaments.

Steady-state models of fiber melt spinning usually consider the distribution of the velocity, temperature and tensile stress of the spun polymer in a single-filament approximation with a predetermined velocity and temperature fields of the gaseous medium. In the case of the pneumatic process with a single row of evenly distributed orifices in a longitudinal spinneret beam, the single-filament model is well-founded because of the relatively low volume occupied by the filaments in the spinning space. The volume density of the filaments is much lower than in the classical processes where considerable aerodynamic interactions take place between the filaments in the cylindrical bundles. In the linear, single-row distribution of filaments in the pneumatic process, the screening effect in the velocity and temperature fields is much reduced and can be omitted.

The model presented in our paper accounts for the effects of viscoelacticity, viscous friction in the bulk of polymer spun at high elongation rates, surface tension and pressure. The model also includes online stress-induced crystallisation and its role in the polymer viscoelasticity and process dynamics.

Model assumptions

In this study, we consider a dynamic model of melt air-drawing in convergent air jets in single-filament approximation. Such approximation is justified for melt blowing from a longitudinal spinneret beam with a single row of orifices. The relatively low volume concentration of the filaments in the spinning space and periodicity of the filaments along the spinning beam allow to consider the process in a single-filament approximation and reduce the modelling to two dimensions. The symmetry of the convergent air jets leads to melt blowing along their centerline. The velocity and temperature fields in a single filament plane, normal for the spinning beam, exhibit severe changes at the air-polymer boundary, accompanied by discontinuity of the material properties, such as density, viscosity, thermal conductivity, etc.

The single-filament model assumes the cylindrical symmetry of the fields in the polymer, reducing the problem to two space variables – the spinning axis z, and the radial distance from the filament axis r. With the thin-filament approximation [14, 21], the model for the stationary processes is reduced to one dimension – with a single variable z. The thin-filament approximation is well-founded because the thickness of filaments in the pneumatic process is usually smaller than that of fibers obtained in classical melt spinning [22-24]. The approximation allows to neglect the radial distribution of the polymer velocity V, temperature T, tensile stress Δp and pressure p. The basis for neglecting the radial distribution of the polymer velocity was found by Ziabicki [2] and Kase [8]. But there is no reliable basis for neglecting the radial gradient of the polymer temperature. Therefore the average temperature on the radial cross-section of the filament is considered a good approximation for thin filaments [14]. Radial distribution of temperature plays a role in the formation of radial structure distribution (molecular orientation, crystallinity). In the modelling of pneumatic melt spinning, axial distributions of the radial-average polymer velocity, temperature, stresses, etc. are considered.

With the single-, thin-filament approach, the air jet velocity, temperature and pressure fields can be approximated by the predetermined fields computed in Part I [19] because any deviation from the fields caused by the presence of a single row of filaments is negligible. Stationary pneumatic melt spinning, used for obtaining uniform fibers in nonwoven, requires stationary boundary conditions for the filaments and stationary air dynamic fields along the melt blowing axis, as well as the stability of the material parameters.

Model equations

A single-, thin-filament model of the stationary air-drawing in melt blowing of nonwovens from crystallising polymer melt is considered, which consists of a set of ordinary, first order differential equations for the z-dependent filament velocity $V(z)$, temperature $T(z)$, tensile stress $\Delta p(z)$, crystallinity $X(z)$ and pressure $p(z)$. The equations result from the mass, force and energy balance equations, the constitutive equation of viscoelasticity and structure development equations, taking into account amorphous orientation and oriented crystallisation. The dynamic conditions active in the process are given by the predetermined velocity, temperature and pressure fields of the air jet, along the filament. The fields were computed in Part I [19] using a turbulent model considering compressible air jets with various initial velocities and fixed initial air temperature at the air slots output.

The mass conservation equation of the polymer filament [4]

$$\frac{\pi D^2(z)}{4}\rho(z)V(z) = W \qquad (1)$$

provides a relation between the local polymer velocity $V(z)$ and its diameter $D(z)$, where $W = const$ is the mass output per single filament, and $\rho(z)$ – the local polymer density. The temperature-dependent density of amorphous izotactic polypropylene reads [25]

$$\rho_a[T(z)] = \frac{10^3}{1.145 + 9.03\times10^{-4}[T(z) - 273]}, \quad \text{in kg/m}^3 \qquad (2)$$

and the crystallinity-dependent density in the two-phase approximation

$$\rho[X(z)] = [1 - X(z)]\rho_a(z) + X(z)\rho_c \qquad (3)$$

where ρ_c – the density of the crystalline component. For isotactic polypropylene $\rho_c = 950$ kg/m^3 [26], and the temperature dependence of the crystalline component density is neglected.

The force balance equation accounts for the local tensile force balancing the inertia, air friction, gravity and surface tension forces in the filament. The take-up force vanishes because the filaments deposit freely onto the collector. The axial gradient of the tensile force $F(z)$ reads [4, 14]

$$\frac{dF}{dz} = W\frac{dV}{dz} + \pi D(z)p_{zr}(z) - \\ + \frac{\pi D^2(z)}{4}\rho(z)g - \frac{\pi}{2}\frac{d}{dz}[\gamma(z)D(z)] \qquad (4)$$

where the terms on the right side are axial gradients of the inertia, air friction, gravity and surface tension forces, respectively. g – the gravity acceleration, $\gamma(z)$ – local surface tension of the polymer. The shear stress resulting from the air friction

$$p_{zr}(z) = \frac{1}{2}\rho_a(z)C_f(z)[V(z) - V_a(z)]^2 \\ sgn[V(z) - V_a(z)] \qquad (5)$$

depends on the local filament diameter $D(z)$ and the difference between the axial velocities of the filament and the air, – $V(z) - V_a(z)$. $C_f(z)$ is the air friction coefficient.

When there is a negative difference between the filament and air local velocity, $V(z) - V_a(z) < 0$, we have a negative axial gradient of the friction force which cumulates the tensile force at the close-to-spinneret part of the filament. This phenomena explains the sharp decrease in filament diameter observed near the spinneret, within a range of 1-2 cm, which is as a consequence of a sharp increase in the elongation rate under the cumulated air friction forces. Therefore the majority of filament attenuation takes place at the short distance of a few centimeters from the spinneret [18]. The mechanisms of the attenuation and settlement of the filament diameter are affected by the dynamic conditions of the process along the melt blowing axis and may be influenced by stress-induced crystallisation, if present. To explain the mechanisms, it is necessary to calculate axial profiles for the polymer velocity, temperature, tensile stress, amorphous orientation factor, and the degree of crystallinity, taking into account oriented crystallisation kinetics.

The air friction coefficient C_f, commonly considered in the modelling of melt spinning and derived by Matsui [27] from experimental correlations, reads

$$C_f = \beta\,\mathrm{Re}_D^{-\alpha} \qquad (6)$$

where α, β are the correlation constants, and the Reynolds number

$$\mathrm{Re}_D(z) = \frac{D(z)|V(z) - V_a(z)|}{\nu_a(z)} \qquad (7)$$

with $\nu_a(z)$ – the local kinematic air viscosity.

Usually, in the modelling of classical melt spinning, one assumes $\beta = 0.37$ and $\alpha = 0.61$ [4, 14, 15, 27]. For the melt blowing process we assume $\beta = 0.78$ and $\alpha = 0.61$, as suggested by Majumdar and Shambaugh [28] where the value of β is typical for the case of the turbulent boundary layer.

The air friction force is a function of the local air density $\rho_a(z)$ and kinematic viscosity of the air $\nu_a(z)$, which depend on the temperature and pressure. The air density along the melt blowing axis z is determined from the relation between the local air pressure $P_a(z)$ and temperature $T_a(z)$

$$\rho_a(z) = const\,\frac{P_a(z)}{T_a(z)} \qquad (8)$$

For dry air and atmospheric pressure, we have $\rho_a(z) = 352.32/T_a(z)$, in kg/m^3 [14]. Thus for a process at the air pressure $P_a(z)$ we have

$$\rho_a(z) = \frac{352.32}{T_a(z)}\,\frac{P_a(z)}{P_{atm}}, \quad \text{in kg/m}^3 \qquad (9)$$

where P_{atm} is the atmospheric pressure.

The dynamic viscosity of dry air at temperature T_a is given by the Sutherland formula [14]

$$\eta_a(T_a) = 1.4663\times10^{-6}\,\frac{T_a^{3/2}}{T_a + 114}, \quad \text{in Pa}\cdot\text{s} \qquad (10)$$

and the local kinematic viscosity of dry air at the pressure $P_a(z)$

$$\nu_a(z) = 4.1618\times10^{-9}\,\frac{T_a^{5/2}(z)}{T_a(z)+114}\,\frac{P_{atm}}{P_a(z)}, \quad \text{in m}^2/\text{s} \qquad (11)$$

The temperature – dependence of the local surface tension of the isotactic polypropylene filament reads [29]

$$\gamma(z) = 2.94\times10^{-2} - 5.6\times10^{-5}\,[T(z) - 296], \quad \text{in N/m.} \qquad (12)$$

The energy conservation equation [4, 14] reads

$$\rho(z)C_p(z)V(z)\frac{dT}{dz} = -\frac{4\alpha^*(z)}{D(z)}[T(z) - T_a(z)] + \rho(z)\Delta h\dot{X}(z) + tr[\mathbf{p}(z)\cdot\dot{\mathbf{e}}(z)] \qquad (13)$$

and expresses the axial gradient of the filament temperature $T(z)$ as controlled by the convective heat exchange between the filament and air jet as well as by the heat of crystallisation and the heat of viscous friction in the polymer bulk, respectively. $C_p(z)$ – specific heat of the polymer, depending on the local filament temperature, α^* – the convective heat exchange coefficient, Δh – the heat of crystallisation per unit mass, $\dot{X}(z)$ the local crystallisation rate, $\mathbf{p}(z)$ and $\dot{\mathbf{e}}(z)$ – the local stress and deformation rate tensors. For isotactic polypropylene we have $\Delta h = 1.65\times10^5$ J/kg [29]. The stress tensor $\mathbf{p}(z)$ is controlled by a constitutive equation of viscoelasticity, and the deformation rate tensor

$$\dot{\mathbf{e}}(z) = \begin{bmatrix} -1/2 & 0 & 0 \\ 0 & -1/2 & 0 \\ 0 & 0 & 1 \end{bmatrix}\frac{dV}{dz} \qquad (14)$$

The linear temperature dependence of the specific heat of the polymer is assumed as

$$C_p(z) = C_{p0} + C_{p1}[T(z) - 273] \qquad (15)$$

For isotactic polypropylene we have $C_{p0} = 1.5358\text{x}10^3$ J/(kg · K), $C_{p1} = 10.13$ J/(kg · K^2) [25].

Model analysis of the dynamic fields of the air jets in Part I [19] indicates that the air flow is coaxial in the melt blowing, and the normal component of the air velocity vanishes along the centerline. The heat exchange coefficient α^* is determined from the correlation between the Nusselt and Reynolds numbers [6, 7]

$$\text{Nu} = 0.42\,\text{Re}_\text{D}^{\,0.334} \qquad (16)$$

where $\text{Nu} = \alpha^* D/\lambda_a$, and λ_a is the thermal conductivity of the air. The numeric parameters in Eq. (16) were confirmed by Bansal and Shambaugh [18] for the melt blowing of polypropylene. The temperature dependence of the air thermal conductivity is given by the Sutherland formula, and for dry air at atmospheric pressure we have

$$\lambda_a(z) = 2.0848\times10^{-3}\,\frac{T_a^{3/2}(z)}{T_a(z)+114}, \quad \text{in J/(m}\cdot\text{s}\cdot\text{K).} \qquad (17)$$

The constitutive equation of viscoelasticity for the uniaxial flow deformation of the polymer defines the uniaxial stress tensor, which is expressed by the axial, p_{zz}, and radial, p_{rr}, stress components. The stress components can be expressed by the tensile stress, $\Delta p = p_{zz} - p_{rr}$, and pressure, $p = -tr\mathbf{p}/3 = -(p_{zz} + 2p_{rr})/3$.

In the steady-state process, the stress tensor is expressed by the local air pressure $P_a(z)$ and extra stress tensor $\sigma(z)$, satisfying the polymer constitutive equation of viscoelasticity with the formula $\mathbf{p}(z) = -P_a(z)\mathbf{I} + \boldsymbol{\sigma}(z)$, where $\mathbf{I}$ is the unit tensor. In the thin-filament approximation, the stress tensor represents the average local stress on the filament cross-section.

The average local tensile stress $\Delta p(z)$ is controlled by the local tensile force $F(z)$

$$\Delta p(z) = \sigma_{zz}(z) - \sigma_{rr}(z) = \frac{F(z)}{\pi D^2(z)}, \qquad (18)$$

and the average local pressure

$$p(z) = P_a(z) + p_{rh}(z) \qquad (19)$$

includes the average rheological pressure associated with the extra stress, $p_{rh}(z) = -tr\boldsymbol{\sigma}(z)/3$.

The product of the local tensile stress $\Delta p(z)$ and the filament elongation rate dV/dz determines the viscous friction heat term in Equation (13)

$$\text{tr}[\mathbf{p}(z)\cdot\dot{\mathbf{e}}(z)] = \Delta p(z)\frac{dV}{dz}. \qquad (20)$$

The Phan-Thien and Tanner constitutive equation of viscoelasticity is used (Equation 21) which introduces two additional material constants: $\in$ – responsible for the non-linear effects, ξ – responsible for the shear thinning effects [30, 31].

For uniaxial flow deformation, Equation 21 is reduced to two scalar equations for the tensile stress $\Delta p(z)$ and rheological pressure $p_{rh}(z)$ (Equations 22 and 23).

For isotactic polypropylene we assume $\in = 0.015$ and $\xi = 0.6$. These values were also used in a computer simulation of the

$$\tau\exp\left(-\in\frac{\tau}{\eta}\,\text{tr}\,\boldsymbol{\sigma}\right)[\dot{\boldsymbol{\sigma}} - (1-\xi)2\boldsymbol{\sigma}\cdot\dot{\mathbf{e}}] + \boldsymbol{\sigma} = 2\eta\exp\left(-\in\frac{\tau}{\eta}\,\text{tr}\,\boldsymbol{\sigma}\right)\dot{\mathbf{e}}, \qquad (21)$$

$$\tau(z)V(z)\frac{d}{dz}\Delta p + \Delta p(z)\exp\left[-3\in\frac{\tau(z)}{\eta(z)}\,p_{rh}(z)\right] = 3\eta(z)\frac{dV}{dz} + \tau(z)(1-\xi)[\Delta p - 3p_{rh}(z)]\frac{dV}{dz}, \qquad (22)$$

$$\tau(z)V(z)\frac{d}{dz}p_{rh} + p_{rh}(z)\exp\left[-3\in\frac{\tau(z)}{\eta(z)}\,p_{rh}(z)\right] = -\frac{2}{3}\tau(z)(1-\xi)\Delta p(z)\frac{dV}{dz}. \qquad (23)$$

Equations 21, 22 and 23.

conventional melt spinning of polypropylene [32].

The shear viscosity is strongly influenced by polymer crystallinity [33] and is expressed by the product of the temperature- and crystallinity-dependent functions [14, 15]

$$\eta(z) = \eta[T(z), X(z)] = \eta_{melt}[T(z)]\,\eta_X[X(z)] \tag{24}$$

The temperature-dependent viscosity of the melt is assumed in the Arrhenius form

$$\eta_{melt}(T) = \begin{cases} \eta_0(M_w)\exp\left(\dfrac{E_a}{kT}\right) & T > T_g \\ \infty & T \le T_g \end{cases} \tag{25}$$

where the pre-exponential factor η_0 depends on the average molecular weight, M_w, E_a is the activation energy, T_g – the glass transition temperature, and k – the Boltzmann constant. For isotactic polypropylene we have $E_a/k = 5.292\times10^3$K and $T_g = 253$K [4,29]. The dependence of η_0 on the average molecular weight M_w known for entangled polymer melts is assumed as [26]

$$\eta_0(M_w) = Const \cdot M_w^{3.4} \tag{26}$$

Using the reference shear viscosity of polymer melt of molecular weight $M_{w,ref}$ at a reference temperature T_{ref}, the pre-exponential factor can be expressed in the form of Equation 27.

In the model, the reference melt viscosity of 3000 Pa · s is chosen for isotactic polypropylene of $M_{w,ref}$ = 300,000 at 220 °C [26].

The effects of crystallisation on polymer viscosity are accounted for by the function η_X derived by Ziabicki [34] from the cross-linking theory

$$\eta_X(X) = \left(1 - \frac{X}{X*}\right)^{-\alpha} \tag{28}$$

where X* is the critical degree of crystallinity at which the polymer solidifies, α – the critical exponent. In the modelling of melt spinning, we usually assume X* = 0.1 and α = 1 [14,15].

The local viscosity of polymer $\eta(z)$ which accounts for the average molecular weight M_w, temperature $T(z)$ and degree of crystallinity $X(z)$, related to the reference melt viscosity, reads (Equation 29).

The local relaxation time $\tau(z)$ is determined from the ratio $\tau(z) = \eta(z) / G(z)$ of the shear viscosity of the polymer and the modulus of elasticity. We assume that the modulus $G(z)$ is dependent on the polymer temperature and crystallinity, which is expressed by the product of functions [35-37]

$$G(z) = G_{melt}[T(z)]\,G_X[X(z)] \tag{30}$$

where the modulus of the melt $G_{melt}[T(z)] = BT(z)$ and the function responsible for the effects of crystallinity $G_X[X(z)] = \exp[3.2X(z) / X_\infty]$ [36, 37]. X_∞ is the maximum degree of crystallinity achievable by the polymer. For isotactic polypropylene we can assume that $X_\infty = 0.55$ [37, 38]. The constant $B = (1 - \xi)^2\,kv$ is proportional to the average number of sub-chains between the entanglements per unit volume, v, irrespective of the polymer molecular weight [30]. Thus the dependence of $\tau(z)$ on the molecular weight results from the dependence of shear viscosity on M_w. We consider the modulus of elasticity at the local temperature $T(z)$ and crystallinity $X(z)$ as expressed by a reference modulus of the melt $G_{melt}(T_{ref})$ at a reference temperature T_{ref}

$$\frac{G(z)}{G_{melt}(T_{ref})} = \frac{T(z)}{T_{ref}}\exp\left[3.2\frac{X(z)}{X_\infty}\right] \tag{31}$$

where $G_{melt}(T_{ref}) = \eta_{melt}(T_{ref}) / \tau_{melt}(T_{ref})$.
The local relaxation time of the polymer is expressed by the reference relaxation time $\tau_{melt}(T_{ref}; M_{w,ref})$ at T_{ref} and average molecular weight $M_{w,ref}$ (Equation 32).

In the model of melt blowing from isotactic polypropylene, we assume that $\tau_{melt}(T_{ref}; M_{w,ref}) = 0.035$ sec at a reference temperature of 220 °C and weight average molecular weight of 300,000. This value was estimated from a relaxation time of 0.04 s reported for polypropylene grade with a shear viscosity of 3420 Pa·s at 210 °C [37].

$$\eta_0(M_w) = \eta_{melt}(T_{ref}; M_{w,ref})\left(\frac{M_w}{M_{w,ref}}\right)^{3.4}\exp\left(-\frac{E_D}{kT_{ref}}\right). \tag{27}$$

$$\frac{\eta(z)}{\eta_{melt}(T_{rel}; M_{w,ref})} = \left(\frac{M_w}{M_{w,ref}}\right)^{3.4}\exp\left[\frac{E_D}{k}\left(\frac{1}{T(z)} - \frac{1}{T_{ref}}\right)\right]\frac{1}{1 - X(z)/0.1}. \tag{29}$$

$$\tau(z) = \frac{\eta(z)}{G(z)} = \tau_{melt}(T_{ref}; M_{w,ref})\frac{T_{ref}}{T(z)}\left(\frac{M_w}{M_{w,ref}}\right)^{3.4}\exp\left[\frac{E_D}{k}\left(\frac{1}{T(z)} - \frac{1}{T_{ref}}\right) - 3.2\frac{X(z)}{X_\infty}\right]\times\frac{1}{1 - X(z)/X*}. \tag{32}$$

$$f_a(z) = \frac{\Delta n_a(z)}{\Delta n_a^0} = \frac{C_{opt}}{\Delta n_a^0}\left[1 - \frac{3}{7}\frac{C_{opt}}{\Delta n_a^0}\Delta p(z) - \frac{1}{7}\left(\frac{C_{opt}}{\Delta n_a^0}\right)^2\Delta p^2(z) - \ldots\right]\Delta p(z). \tag{33}$$

$$\dot{X}(z) = V(z)\frac{dX}{dz} = n\left(1 - \frac{X(z)}{X_\infty}\right)\left[-\ln\left(1 - \frac{X(z)}{X_\infty}\right)\right]^{1-1/n}K_{st}(z). \tag{34}$$

$$K_{st}(z) = K_{st}(T, \Delta p) = \begin{cases} K_{\max}\exp\left[-4\ln 2\dfrac{(T(z) - T_{\max})^2}{D_{1/2}^2}\right]\exp\left[Af_a^2(z)\right] & T(z) < T_m^0 \\ 0 & T(z) \ge T_m^0 \end{cases}. \tag{35}$$

Equations 27, 29, 32, 33, 34 and 35.

Structure evolution equations concern the development of molecular orientation and the degree of crystallinity under uniaxial flow deformation. Molecular orientation is considered using the following non-linear stress-optical formula [15] between the amorphous orientation factor $f_a(z)$, or birefringence $\Delta n_a(z)$, and the local tensile stress Δp (Equation 33). Δn_a^0 denotes the birefringence of perfectly oriented amorphous polymer, C_{opt} – the stress-optical coefficient. For isotactic polypropylene $\Delta n_a^0 = 60.0\times10^{-3}$ and $C_{opt} = 9.0\times10^{-10}$m^2/N [39].

The stress-induced crystallisation rate under non-isothermal conditions is determined from the Avrami equation and reads [40, 41] (Equation 34) where $K_{st}(z)$ is the crystallisation rate function dependent on the temperature and tensile stress. The following Gaussian dependence on temperature and exponential dependence on the amorphous orientation factor, f_a, of the crystallisation rate function is assumed as [4] (Equation 35).

For isotactic polypropylene we have $K_{max} = 0.55$ s^{-1}, $T_{max} = 338$ K, $D_{1/2} = 60$ K, and the equilibrium melting temperature $T_m^0 = 453$ K [4]. The factor A is reported only for PET [42], with the values in the range 100 – 1000.

Boundary conditions

The mathematical model of non-woven melt blowing by crystallising viscoelastic polymer consists of five first order differential equations for axial profiles of the polymer velocity $V(z)$, temperature $T(z)$, tensile force $F(z)$, rheological pressure $p_{rh}(z)$, and the degree of crystallinity $X(z)$. The equations derived from Equations 1, 4, 13, 22, 23, 34 assume a general form $df_i / dz = g_i[V(z), T(z), F(z), p_{rh}(z), X(z)]$ where $f_i(z)$ are the axial profiles, $g_i[\cdot]$ – functions dependent on the axial profiles. Initial values $f_i(z = 0)$ of the profiles are defined for the initial polymer velocity $V(z = 0) = V_0$, temperature $T(z = 0) = T_0$, crystallinity $X(z = 0) = 0$ and the rheological pressure $p_{rh}(z = 0) = 0$. The value of $F(z = 0)$ does not exist because it is difficult to control the initial force directly. In the modelling of classical melt spinning, the initial tensile force is adjusted to the take-up velocity by the inverse method. In the melt blowing of nonwovens, the filaments deposit freely onto the collector; however, it is difficult to control the take-up velocity. The condition of the vanishing tensile force on the collector allows to determine the initial force by adjusting it by the inverse method.

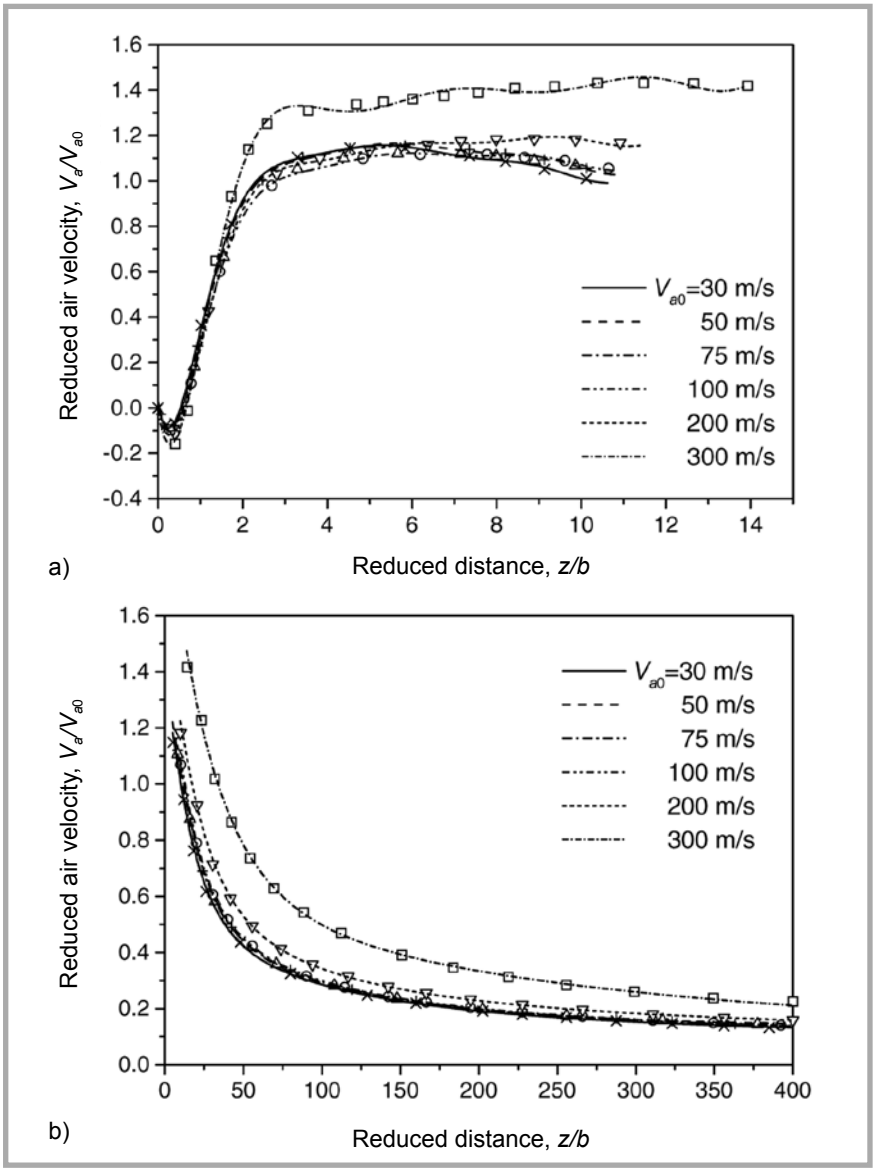

Figure 1. *Reduced air jet velocity $V_a(z / b) / V_{a0}$ vs. the distance from the spinneret z/b (lines), matching the computer simulation data (points) [19] for various initial air velocities, a) short distances; b) longer distances from the spinneret. T_{a0} = 300 °C.*

Axial distributions of the air velocity, temperature and pressure along the filament between the initial point, $z = 0$, and collector, $z = L$, also constitute some kind of boundary conditions which control the melt blowing dynamics. The predetermined air jet conditions along the filament axis were computed in Part I [19] on the basis of the $k – \varepsilon$ aerodynamic model for convergent air jets blown from a dual slot die. The centerline distribution of the air jet conditions was obtained form the simulation as a set of numerical data; however, for the modelling they should be represented by analytical formulae.

For a satisfactory analytical approximation of the axial profiles of the air velocity $V_a(z)$, temperature $T_a(z)$ and pressure $P_a(z)$, the axial distance is divided into two ranges – nearby the spinneret $0 – z_1$ range, and the remaining $z_1 – L$ range. In the first range, the simulation data representing axial profiles of the air fields are fitted into the following functions using the polynomial regression method

$$f_i^{air}\left(\frac{z}{b}\right) = B_0 + \sum_{n=1}^{N} B_n \left(\frac{z}{b}\right)^n,\ 0 \le z \le z_1 \quad . \tag{36}$$

The functions $f_i^{air}(z / b)$ are fields profiles reduced by the initial values vs. the axial

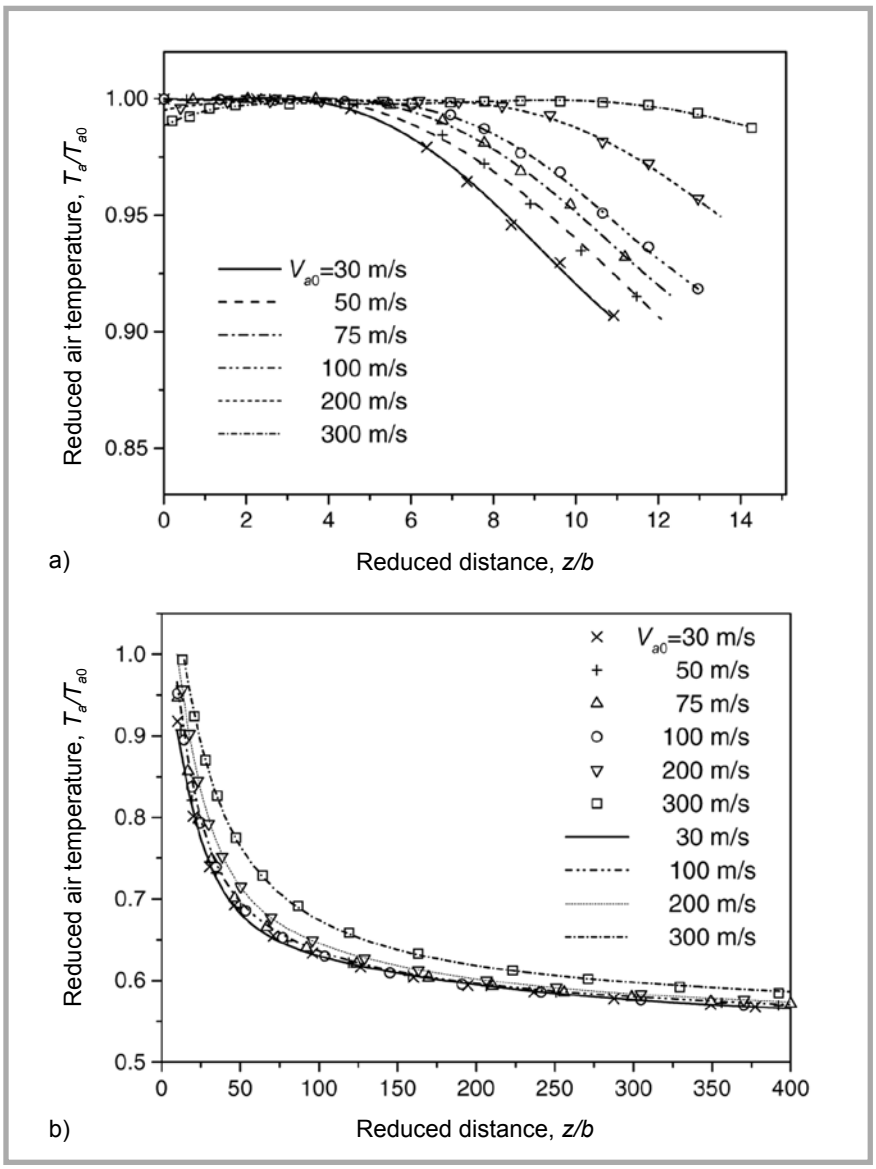

Figure 2. *Reduced air jet temperature $T_a(z / b) / T_{a0}$ vs. the distance from the spinneret z/b (lines), matching the computer simulation data (points) [19] for various initial air velocities a) short distances; b) longer distances from the spinneret. T_{a0} = 300 °C.*

distance reduced by the width of the air die at the output, z/b. It concerns air velocity reduced by its initial velocity, $V_a(z/b)/V_{a0}$, reduced air temperature, $T_a(z/b)/T_{a0}$, and reduced air pressure, $P_a(z/b)/P_{a0}$. For the air die considered in [19,20] we have $b = 0.5$ mm.

Within the remaining $z_1 - L$ range, the reduced air field profiles are approximated using the third order exponential decay fit

$$f_i^{air}\left(\frac{z}{b}\right) = C_0 + \sum_{n=1}^{3} C_n \exp\left(-\frac{z}{t_n b}\right), \quad z_1 < z \le L \tag{37}$$

The fit coefficients B_n, C_n and t_n for the air velocity and temperature profiles are presented in ***Tables 1 and 2*** (see pages 23 and 24) for various initial air velocities: 30, 50, 75, 100, 200 and 300 m/s, at a fixed initial air temperature of 300 °C, as well as the division point z_1 and the non-linear regression fit parameters R. The air pressure along the spinning axis decreases to an atmospheric value within the $0 - z_1$ range. The fit coefficients B_n and the non-linear regression fit parameters R to the air pressure data are listed in ***Table 3*** (see pages 24). The fit functions are illustrated in ***Figures 1-3***, where the points represent computer simulation data [19,20].

The axial profiles of the reduced air velocity ***(Figures 1)*** almost overlap at not too high initial air velocities: up to 100 m/s, and differ more at higher initial air velocities. At the short distance range of $z < z_1 = 10b = 5$ mm, the maximum for the air velocity is predicted as well as a reverse air flow within a very narrow range of the order of slot width b at the spinneret face. At higher axial distances, $z > z_1 = 10b$, and at not too high initial air velocities (up to 75 m/s), the reduced air velocity profiles follow the power law decay

$$\frac{V_a(z)}{V_{a0}} = 4.110\left(\frac{z}{b}\right)^{-0.572} \quad \text{for } z_1 < z \le L \tag{38}$$

with the fit parameter $R < 0.9997$. A similar power law decay was reported by Krutka et al. [43] for a computer simulation of dual air jets based on Reynolds stress model. At initial air velocities 200 m/s or higher, the air velocities computed in [19] deviate from the power low, Eq. (38).

Contrary to the velocity profiles at not high initial air velocities, the temperature profiles at short distances, $z < z_1$, do not overlap **(*Figure 2.a*)** and increase with a rising V_{a0}. At higher distances, $z > z_1$, the temperature profiles show exponential decay **(*Figure 2.b*)** and do not fit any power law with reasonable accuracy.

The air pressure profiles show an increase to the maximum, which is more easily distinguishable at the highest initial air velocities. Next they are discharged to the atmospheric pressure within a very narrow distance range of the order of $3b$ from the die. The air pressure axial profiles are presented in ***Figure 3***, where the polynomial regression matches the simulation data [19, 20].

Summary

In this article, we propose a single-filament model for the stationary melt blowing of nonwovens from isotactic polypropylene in the thin-filament approximation. The model equations account for the effects of viscoelasticity and stress-induced crystallisation in the rheological behaviour of polymer during processing. The predetermined air velocity, temperature and pressure fields of the air along the blown filament are assumed, computed for different initial air velocities in Part I [19]. The air fields active along the processing axis are approximated by analytical fit formulae. The model can be easily applied to melt blowing processes involving other crystallising polymers, as well as other predetermined air dynam-

ic fields. Axial profiles of the dynamic functions computed from the model for the melt blowing of nonwovens from isotactic polypropylene will be discussed in Part III [44] of the publication series, and some of them have been presented in [20].

Acknowledgement

This paper resulted from research supported by Research Grant Nr 3 T08E 08628 from the State Committee for Scientific Research, Poland.

References

1. *Ziabicki A., Kędzierska K., Kolloid Z., 1960, 171, 51.*
2. *Ziabicki A., Kolloid Z., 1961, 175, 14; 1961, 179, 116.*
3. *Ziabicki A., in: "Man Made Fibres. Science and Technology", H. Mark, S. Atlas, E. Cernia Eds., Interscience, NewYork 1967, p. 56.*
4. *Ziabicki A., "Fundamentals of Fibre Formation", J. Wiley, London 1976.*
5. *Andrews E.H., Brit. J. Appl. Phys., 1959, 10, 39.*
6. *Kase S., Matsuo T., J. Polymer Sci., 1965, A-3, 2541.*
7. *Kase S., Matsuo T., J. Appl. Polymer Sci., 1967, 11, 251.*
8. *Kase S., J. Appl. Polymer Sci., 1974, 18, 3267.*
9. *Yasuda H., in: "High Speed Melt Spinning", A. Ziabicki, H. Kawai Eds., J. Wiley, New York 1985, p. 363.*
10. *Ishihara H., Hayashi S., Ikeuchi H., International Polymer Processing, 1989, 4, 91.*
11. *Matsui M, in: "High Speed Melt Spinning", A. Ziabicki, H. Kawai Eds., J. Wiley, NewYork 1985, p. 137.*
12. *Shimizu J., Okui N., Kikutani T., in: "High Speed Melt Spinning", A. Ziabicki, H. Kawai Eds., J. Wiley, NewYork 1985, p. 173.*
13. *Katayama K., Yoon M.G., in: "High Speed Melt Spinning", A. Ziabicki, H. Kawai Eds., J. Wiley, NewYork 1985, p. 207.*
14. *Ziabicki A., Jarecki L., Wasiak A., Comput. Theoret. Polymer Sci., 1998, 8, 143.*
15. *Jarecki L., Ziabicki A., Blim A., Comput. Theoret. Polymer Sci., 2000, 10, 63.*

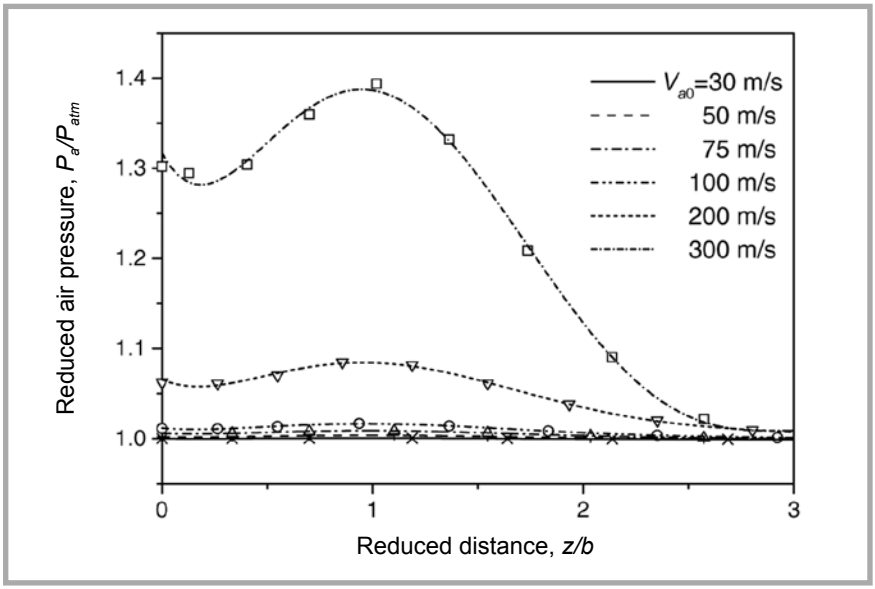

Figure 3. *Reduced air pressure $P_a(z / b) / P_{atm}$ vs. the distance from the spinneret z/b (lines) matching the computer simulation data (points) [19] for various initial air velocities. T_{a0} = 300 °C.*

Table 1. *Fit coefficients B_n, C_n, t_n and fit parameter R of the reduced air velocity $V_a(z / b) / V_{a0}$, Equations (36, 37), matching the computed data [19] for various initial air velocities V_{a0}. Two ranges of z/b considered. T_{a0} = 300 °C.*

V_{a0}	30 m/s	50 m/s	75 m/s	100 m/s	200 m/s	300 m/s
z/b:	**0-10**	**0-10**	**0-10**	**0-10**	**0-10**	**0-14**
B_0	0.01432016	0.01341548	0.02652139	0.0158094	0.01852046	–0.01793676
B_1	–0.94042894	–0.96953629	–1.03015674	–0.99768896	–1.1075811	–1.12594769
B_2	2.47692165	2.45905054	2.4860587	2.41519221	2.53944931	2.54260332
B_3	–1.70053897	–1.65567181	–1.66266322	–1.60754842	–1.63434399	–1.47461909
B_4	0.59915931	0.57246156	0.057377515	0.55191824	0.54123882	0.42783846
B_5	–0.12418755	–0.11636277	–0.11657096	–0.11159957	–0.10531489	–0.07173064
B_6	0.01571995	0.01443584	0.01446372	0.01378932	0.01250371	0.00725798
B_7	–0.00119511	–0.00107505	–0.00107765	–0.00102371	-8.911×10^{-4}	-4.37489×10^{-4}
B_8	5.01361×10^{-5}	4.41579×10^{-5}	4.42932×10^{-5}	4.1946×10^{-5}	3.50273×10^{-5}	1.44663×10^{-5}
B_9	-8.91999×10^{-7}	-7.68938×10^{-7}	-7.7185×10^{-7}	-7.28979×10^{-7}	-5.83698×10^{-7}	-2.01989×10^{-7}
R	0.999584	0.999542	0.999565	0.999562	0.999366	0.998167
z/b:	**> 10**	**> 10**	**> 10**	**> 10**	**> 10**	**> 14**
C_0	0.06375957	0.13621931	0.0849706	0.08828576	0.08515634	0.12045473
C_1	0.90828826	0.94398992	0.95166243	0.97416913	1.03300019	1.0438441
t_1	16.31131548	18.3741266	13.87263141	14.9621545	19.28219258	34.14203298
C_2	0.33806314	0.26623395	0.39119955	0.37332762	0.39305135	0.48617114
t_2	84.6274745	99.64100941	56.64176188	62.06884512	79.00939849	238.99485802
C_3	0.14087167	0.11663971	0.19885598	0.18777833	0,17541927	0.43340948
t_3	521.62940731	131.00942446	298.21411309	304.87658541	443.1517509	17.95289425

Table 2. *Fit coefficients B_n, C_n, t_n and fit parameter R of the axial profiles of the reduced air temperature $T_a(z / b) / T_{a0}$, Equations (36, 37), matching the computed data [19] for various initial air velocities V_{a0}. Two ranges of z/b considered. T_{a0} = 300 °C.*

V_{a0}	30 m/s	50 m/s	75 m/s	100 m/s	200 m/s	300 m/s
z/b:	**0-10**	**0-10**	**0-10**	**0-10**	**0-10**	**0-14**
B_0	1.00021409	0.99876227	0.99980519	0.99998897	0.99496568	0.98837895
B_1	–0.00186696	0.00126654	–0.00146766	-4.37792×10^{-4}	0.00431719	0.00879604
B_2	0.00174891	3.11019×10^{-4}	9.99839×10^{-4}	-1.63927×10^{-4}	–0.00191776	–0.00293472
B_3	-4.41715×10^{-4}	-1.75674×10^{-4}	-1.45404×10^{-4}	1.6696×10^{-4}	4.00109×10^{-4}	4.36289×10^{-4}
B_4	2.05631×10^{-5}	7.2975×10^{-6}	-3.90932×10^{-6}	-3.18244×10^{-5}	-3.63374×10^{-5}	-2.85515×10^{-5}
B_5	0.0	0.0	5.06442×10^{-7}	1.33168×10^{-6}	1.04445×10^{-6}	6.54909×10^{-7}
R	0.999523	0.998719	0.999238	0.998826	0.998408	0.984518
z/b:	**> 10**	**> 10**	**> 10**	**> 10**	**> 10**	**> 14**
C_0	0.55183812	0.5520943	0.56727286	0.54739008	0.54508819	0.56420689
C_1	0.31587112	0.33029406	0.30431692	0.41319373	0.44709533	0.23657022
t_1	20.51694319	20.80601806	19.03390321	13.30996441	18.07594706	54.25398636
C_2	0.1332654	0.13864468	0.19519456	0.16261634	0.14417173	0.104872
t_2	177.40898616	175.59117926	8.48574882	53.54411096	84.35321814	257.36693839
C_3	0.07189264	0.11341208	0.15839395	0.08923285	0.06907785	0.33158856
t_3	12.91394124	11.30678194	114.93830485	294.91362213	431.26957148	17.63642493

Table 3. *Fit coefficients B_i and fit parameter R of the axial profiles of the reduced air pressure $P_a(z / b) / P_{a0}$, Equation (36), matching the computed data [19] for various initial air velocities V_{a0}. T_{a0} = 300 °C.*

V_{a0}	30 m/s	50 m/s	75 m/s	100 m/s	200 m/s	300 m/s
z/b:	**0-10**	**0-10**	**0-10**	**0-10**	**0-10**	**0-14**
B_0	1.00004504	1.00214566	1.00596521	1.01171483	1.06550167	1.31650855
B_1	–0.00192678	–0.00536512	–0.01133084	–0.02000098	–0.09901194	–0.42417518
B_2	0.00871069	0.02334346	0.0480091	0.08316157	0.38717131	1.55348243
B_3	–0.01017822	–0.02693927	–0.05491905	–0.09460418	–0.43154981	–1.62858499
B_4	0.00499676	0.01307988	0.02643967	0.04528379	0.20179267	0.68809063
B_5	–0.00112863	–0.00292268	–0.00585672	–0.00996858	–0.04320812	–0.12741137
B_6	9.71253×10^{-5}	2.48887×10^{-4}	4.94392×10^{-4}	8.36025×10^{-4}	0.00351215	0.00847884
R	0.998674	0.998550	0.998435	0.998354	0.997826	0.998043

16. *Chen T., Huang X., Textile Res. J., 2003, 73, 651.*
17. *Chen T., Wang X., Huang X., Textile Res. J., 2005, 75, 76.*
18. *Bansal V., Shambaugh R.L., Ind. Eng. Chem. Res., 1998, 37, 1799.*
19. *Zachara A., Lewandowski Z., Fibres and Textiles in Eastern Europe, 2008, 16, 17.*
20. *Lewandowski Z., Ziabicki A., Jarecki L., Fibres and Textiles in Eastern Europe, 2007, 15, 77.*
21. *Petrie C.J.S., "Elongational Flows", Pitman, London, 1979.*
22. *Farer R., Seyman A.M., Ghosh T.K., Grant E., Batra S.K., Textile Res. J., 2002, 72, 1033.*
23. *Farer R., Batra S.K., Glosh T.K., Grant E., Seyam A.M., Internat. Nonwovens J., 2003, Spring, 36.*
24. *Moore E.M., Papavassiliou D.V., Shambaugh R.L., Internat. Nonwovens J., 2004, Fall, 43.*
25. *Zieminski K.F., Spruiell J.E., Synthetic Fibers, 1986, 4, 31.*
26. *van Krevelen D.W., "Properties of Polymers", Elsevier, Amsterdam 2000, pp. 86, 463, 469.*
27. *Matsui M., Trans. Soc. Rheol., 1976, 20, 465.*
28. *Majumdar B., Shambaugh R.L., J. Rheol., 1990, 34, 591.*
29. *Mark J.E., "Physical Properties of Polymers, Handbook", AIP Press, New York 1996, pp. 424, 670.*
30. *Larson R.G., "Constitutive Equations for Polymer Melts and Solutions", Butterwoths, Boston 1988, p.171.*
31. *Phan-Thien N., Rheol J., 1978, 22, 259.*
32. *Shin D.M., Lee J.S., Jung H.W., Hyun J.Ch., Korea-Australia Rheology J., 2005, 17, 63.*
33. *Ziabicki A., Jarecki L., Sorrentino A., e-Polymers, 2004, 072.*
34. *Ziabicki A., J. Non-Newtonian Fluid Mech., 1988, 30, 157.*
35. *Joo Y.L., Sun J., Smith M.D., Armstrong R.C., Brown R.A., Ross R.A., J. Non-Newtonian Fluid Mech., 2002, 102, 37.*
36. *Patel R.M., Bheda J.H., Spruiell J.E., J. Appl. Polymer Sci., 1991, 42, 1671.*
37. *Lee J.S., Shin D.M., Jung H.W., Hyun J.C., J. Non-Newtonian Fluid Mech., 2005, 130, 110.*
38 *Kolb R., Sefert S., Stribeck N., Zachmann H. G., Polymer, 2000, 41, 1497.*
39. *Samuels R. J., "Structured Polymer Properties", J. Wiley, New York 1974, p. 58.*
40. *Ziabicki A., Colloid Polymer Sci., 1974, 252, 207.*
41. *Ziabicki A., Colloid Polymer Sci., 1996, 274, 209.*
42. *Alfonso G.C., Verdona M.P., Wasiak A., Polymer 1978, 19, 711.*
43. *Krutka H.M., Shambaugh R.L., Papavassiliou D.V., Ind. Eng. Chem. Res., 2003, 42,5541.*
44. *Jarecki L., Lewandowski Z., Fibres and Textiles in Eastern Europe, accepted for publication, Vol. 17 Nr 1, 2009.*

❑ ***Received 8.11.2007 Reviewed 13.12.2007***